

1 **Disproportionate increase in freshwater methane emissions induced**
2 **by experimental warming**

3 **Authors:** Yizhu Zhu¹, Kevin J Purdy², Özge Eyice¹, Lidong Shen^{1,3}, Sarah F Harpenslager^{1,4}, Gabriel
4 Yvon-Durocher⁵, Alex J. Dumbrell⁶, Mark Trimmer^{1*}

5 **Affiliations:**

6 ¹School of Biological and Chemical Sciences, Queen Mary University of London, London, E1 4NS, UK.

7 ²School of Life Sciences, University of Warwick, Coventry, CV4 7AL, UK.

8 ³Institute of Ecology, School of Applied Meteorology, Nanjing University of Information Science and
9 Technology, Nanjing 210044, China.

10 ⁴Leibniz Institute of Freshwater Ecology and Inland Fisheries (IGB), Department of Ecosystem Research,
11 12587, Berlin, Germany.

12 ⁵Environment and Sustainability Institute, University of Exeter, Penryn Campus, Penryn, Cornwall, TR10
13 9FE, UK.

14 ⁶School of Life Sciences, University of Essex, Colchester, Essex, U.K. CO4 3SQ.

15 *Correspondence to: Mark Trimmer m.trimmer@qmul.ac.uk

16

17 Words in main text: 2148 and words in Methods: 3374

18 Words in introductory paragraph: 150

19 Figures: 5 and Extended data figures: 3

20 References in main text: 37 and references in Methods only: 19

21 **Main text:**

22 **Net emissions of the potent greenhouse gas methane from ecosystems represent the balance**
23 **between microbial methane production (methanogenesis) and oxidation (methanotrophy), each**
24 **with different sensitivities to temperature. How this balance will be altered by long term global**
25 **warming, especially in freshwaters that are major methane sources, remains unknown. Here we**
26 **show that experimental warming of artificial ponds over 11 years drives a disproportionate**
27 **increase in methanogenesis over methanotrophy that increases the warming potential of the gases**
28 **they emit. Increased methane emissions far exceed temperature-based predictions, driven by shifts**
29 **in the methanogen community under warming, while the methanotroph community was conserved.**
30 **Our experimentally induced increase in methane emissions from artificial ponds is, in part,**
31 **reflected globally as a disproportionate increase in the capacity of naturally warmer ecosystems to**
32 **emit more methane. Our findings indicate that as Earth warms, natural ecosystems will emit**
33 **disproportionately more methane in a positive feedback warming loop.**

34 Methane makes a large contribution to climate change and methane concentrations are increasing
35 in the atmosphere^{1,2}. A significant proportion (~42% of all natural and anthropogenic sources) of methane
36 is emitted from freshwaters (wetlands, lakes and rivers) that make a disproportionately large contribution
37 to the global methane budget for their comparatively modest sizes^{3,4}. Methane production by
38 methanogens and its oxidation by methanotrophs drive the biological methane cycle, with the balance
39 between the two regulating net methane emissions⁵. Methanogenesis is very sensitive to temperature⁶, e.g.
40 an increase of 10°C would drive a 4.0-fold increase in methane production^{7,8}, while, in contrast,
41 methanotrophy⁹, being more strongly substrate limited, is less sensitive to temperature¹⁰. Due to these
42 different physiological responses to temperature, long-term warming might alter the structure of
43 methanogen and methanotroph communities, disturbing the balance between the two processes and
44 ultimately increasing methane emissions^{11,12}.

45 Linking microbial community structure to ecosystem-level processes is a major theoretical
46 challenge¹³. Therefore, measuring microbial community characteristics such as functional diversity^{12,14},
47 gene abundance¹⁵, growth efficiency¹⁶ and thermodynamic constraints¹⁷ is essential to determine how
48 microbial community structure influences ecosystem-level processes¹³. This need is particularly acute at
49 the long-term time-scale in the methane cycle as previous investigations into the effect of warming on
50 methanogenesis and methanotrophy were typically limited to less than 1 year which may have masked the
51 effects of any shifts in the microbial communities^{12,18,19}. Key unanswered questions under current climate
52 warming scenarios remain: **1**, does long-term warming (>10 years) alter the balance between
53 methanogenesis and methanotrophy; and **2**, how do any changes in the methane-related microbial
54 communities affect net methane emissions?

55 We answered these questions by studying the long-term effects of warming on freshwater
56 ecosystem-level methane cycling in 20 well-established, artificial ponds^{20,21}, half of which have been
57 heated to 4°C above ambient since September 2006. Each pond is 1.8m wide, has a surface area of 2.5m²
58 and approximately 50cm of water over 10cm of sandy sediments (Extended Data Figure 1). After 11
59 years of warming, frequent measurements (three times daily) revealed an ongoing divergence in methane
60 emissions from the surface of the ponds to the atmosphere between our warmed and ambient ponds (Fig.
61 1a and Extended Data Fig. 2). Annual methane emissions are now 2.4-fold higher under warming and far
62 in excess of the 1.7-fold increase predicted (*see* equation 2) through a simple physiological response to
63 higher temperatures alone^{7,8}. Here methane emissions are dominated by diffusion (98.8%) rather than
64 ebullition (1.2%)²², probably because of the relatively shallow sediments in our ponds (~ 10 cm) but the
65 magnitude of ebullition is similarly amplified under warming (Supplementary Fig. 1). Even though the
66 ponds are net sinks for CO₂^{20,21}, the ratio of CH₄ to CO₂ emitted at night has also increased by 1.8-fold
67 under warming, increasing the global warming potential (GWP) of the carbon-gases emitted overall (Fig.
68 1b)². These long-term observations underline the potential of climate-warming to continually amplify
69 methane emissions from freshwaters; a prediction that is supported by a meta-analysis showing an

70 increase in the capacity of wetlands, grasslands and soils to emit methane in regions with higher annual
71 average temperatures (Fig. 1c and *see* Supplementary Table 1 for sites included) and from observations of
72 increased methane emissions, driven by a fundamental change in the ecosystem, along a natural gradient
73 of thawing permafrost²³. These observations clearly show that the methane cycle does not respond to
74 warming through a simple physiological response, but rather to shifts in the structure and/or activity of
75 the overall methane related microbial community. This more complex response to warming will affect
76 how we predict changes in methane emissions under climate warming scenarios.

77 To rationalise both the disproportionate increases in CH₄ emissions and ratio of CH₄ to CO₂ after
78 11 years of warming, we measured the methane production capacity of the pond sediments at the same
79 temperature (15°C) in the laboratory in controlled microcosms. Warmed pond sediments produced 2.5-
80 fold more methane than their ambient controls (*post-hoc* pairwise comparisons: $p < 0.05$, Fig. 2a,b) for the
81 same quality of carbon (carbon turnover k , t -statistic, $p = 0.053$, *see* also C to N ratio in Supplementary
82 Table 2). The potential of sediments to produce methane increased equally in both the warmed and
83 ambient ponds as carbon quality also increased (Fig 2b, $p = 0.4$). Warming has, however, stepped-up the
84 fraction of carbon turned-over to methane because methanogens are now 1.5-fold more abundant in the
85 warmed ponds (qPCR of the *mcrA* gene, Fig. 2c, circles, t -statistic, $p < 0.05$) and, importantly,
86 methanogens in the long-term warmed ponds appeared to be ~60% more efficient at making methane too
87 (Fig. 2c, triangles). This increase in methanogen efficiency explains the disproportionate increase in
88 methane emissions (Fig. 1a) and, by increasing the ratio of CH₄ to CO₂ produced in the sediment by 3-
89 fold (t -statistic, $p < 0.001$, Fig. 2d), also accounts for the increased ratio of CH₄ to CO₂ emitted to the
90 atmosphere at night (Fig. 1b). These increases are, however, hard to rationalise without a fundamental
91 change to the structure of the methanogen community.

92 In freshwater sediments, methane is produced predominantly by acetoclastic and
93 hydrogenotrophic methanogenesis²⁴. Theoretically these two types of methanogenesis have stoichiometric
94 equivalence and complete glucose degradation should produce CH₄ and CO₂ in a 1:1 ratio²⁵, with 33%

95 CH₄ from hydrogenotrophy and 67% CH₄ from acetoclastic methanogenesis (ref. 24, 25 and *see*
96 Supplementary Discussion). Just as in our pond sediments (Fig. 2d), however, this idealised 1:1 ratio is
97 seldom found with deviations from 1:1 being ascribed to differences in organic matter oxidation state, pH
98 or organic matter quality²⁷⁻²⁹ that simply do not apply to our ponds. Alternatively, we would argue that
99 the proportion of available H₂ flowing to methane increases under warming^{17,28} (*see* Supplementary
100 Discussion) and that the increase in both methanogen efficiency and CH₄ to CO₂ ratios (Fig. 2c, 2d and 1b)
101 suggested a shift towards hydrogenotrophic methanogenesis with long-term warming. We tested this
102 hypothesis by analysing the methanogen communities and, in accordance, identified significant shifts in
103 two dominant hydrogenotrophic genera between the warmed and ambient ponds (Fig. 3a and b and
104 Supplementary Tables 3 and 4) but no significant changes in any other methanogens (e.g. acetoclastic
105 genera). Specifically, the relative abundance of *Methanobacterium* increased significantly from 8.5% to
106 13.2% of the methanogen community, whereas, in contrast, *Methanospirillum* decreased from 31.3% to
107 22.7% between the ambient and warmed ponds, respectively (adjusted *p*-value <0.01, Fig. 3b). After 11
108 years of warming methanogen diversity was conserved (Supplementary Fig. 2) but marginal changes in
109 the relative abundance of *Methanobacterium* and *Methanospirillum* and other minor changes within the
110 community (with 4 hydrogenotrophic genera increasing in relative abundance and two new genera
111 appearing in the warmed ponds; Supplementary Table 4) appeared to be linked to the increased
112 contribution from hydrogenotrophic methanogenesis – increasing methane production and the ratio of
113 CH₄ to CO₂ emitted. Other ecosystems, such as thawing peat permafrost, also show increased methane
114 emissions on warming²³ but these are linked to fundamental successional changes in the methanogen
115 community that match successional changes in the ecosystem. Yet, our freshwater ponds show that subtle
116 shifts in the methanogen community can produce substantial changes to the methane emissions of these
117 ecosystems under warming that would suggest natural freshwater systems are likely to be capable of
118 responding in a similar manner (Fig 1c, ref. 7 and 28).

119 We performed further incubations with the addition of hydrogen and acetate (Fig. 3c) to identify a
120 mechanism for these changes in the methanogen community and measured a disproportionate increase in
121 methane production with hydrogen in the warmed pond sediments (Fig. 3c). Further short-term
122 temperature manipulations also clearly showed that hydrogenotrophic methanogenesis was the most
123 sensitive to temperature, with an apparent activation energy of 1.40 eV for H₂ compared to 0.7 eV for the
124 controls (*post-hoc* pairwise comparisons: $p < 0.001$, Fig. 3d). Thus, warming makes hydrogenotrophic
125 methanogenesis more favourable, providing a mechanism to drive the shift towards a more
126 hydrogenotrophic methanogenesis due to warming.

127 Short-term (<3 months) experiments in wetlands have shown that the relative contribution of
128 hydrogenotrophic methanogenesis decreases at lower temperatures^{17,28,30-32}. Conversely, hydrogenotrophy
129 dominates in warmer freshwater environments and a community meta-analysis identified strong selection
130 for hydrogenotrophic methanogens in warm environments³³⁻³⁵. Here for the first time we demonstrate
131 experimentally that long-term warming of a freshwater community favours hydrogenotrophic over
132 acetoclastic methanogenesis, altering both the efficiency and structure of the methanogen community to
133 increase the ratio of produced and emitted CH₄ to CO₂ (Fig. 3a, 3b, 2d and 1b). Our observations reflect
134 subtle changes in the structural and functional ecology of shallow ponds in stark contrast to the major
135 changes seen in hydrology, vegetation, organic matter quality and pH along a natural gradient of thawing
136 permafrost²³, where increases in methane emissions run alongside major alteration to the methanogen
137 community. Further, the predictable physiological increase in methane emissions seen after 1 year of
138 experimental warming in peatland soils¹⁹, mirrors what we first observed in our ponds³⁶ - if ongoing
139 warming sets peat on a similar trajectory, as our meta-analysis suggests, then we would predict
140 disproportionate increases in methane emissions from peatlands too.

141 The balance between methane production and its oxidation controls the net emission of methane.
142 We used similar laboratory microcosm incubations to those described above to investigate whether long-
143 term warming enhanced methane oxidation to the same magnitude as methane production. In contrast to

144 methane production, however, we found the sediments' capacity to oxidise methane to be the same in
145 both our warmed and ambient ponds (likelihood ratio test: $p=0.93$, Fig. 4a). The methanotrophs did have
146 a strong kinetic potential to oxidise more methane and warming-induced increases in methane
147 concentrations in the ponds (2.1-fold, Supplementary Table 2), were reflected in increased methane
148 oxidation activity in the laboratory (1.9-fold, *see* equation (7) for Michaelis-Menten model). Similarly,
149 while the temperature sensitivity of methane oxidation – in the laboratory – was the same in both warmed
150 and ambient pond sediments (likelihood ratio test: $p=0.24$, Fig. 4b), the 4°C of warming *in situ* would
151 increase methane oxidation activity too (i.e., 1.4-fold increase with the common activation energy of 0.57
152 eV in equation (2)). Altogether, higher methane concentrations and the 4°C of warming would increase
153 the methane oxidation capacity of the warmed ponds by 2.6-fold (Supplementary Table 2). Further, as
154 methanotrophic activity is confined to a thin, oxic zone at the sediment surface³⁷, which was ~40%
155 shallower in the warmed ponds (Supplementary Fig. 3), there would have been an oxygen effect too.
156 Combined, the methane kinetic, temperature and oxygen-penetration effects (1.9-, 1.4- and 1.4- fold,
157 respectively) would drive 3.6-fold greater methane oxidation activity in the warmed ponds (*see*
158 Supplementary Table 2 and further discussion there in) that ultimately attenuated ~95% of the extra
159 methane production under warming but not the 98% required to prevent increased methane emissions.
160 Which poses the question: why might methanotrophs not be able to keep-up with methanogens under
161 warming?

162 Methanotroph abundance did increase in the warmed ponds but not enough (2.45-fold *v.s.* 2.67-
163 fold required, *see* Supplementary Table 2) to offset the greater warming-induced methane production. As
164 a proxy for their growth-efficiency¹⁶ we measured the fraction of methane assimilated into methanotroph
165 biomass (carbon conversion efficiency i.e., CCE) in the laboratory. Accordingly, methanotroph CCE was
166 indistinguishable between the warmed and ambient sediments, however, methanotroph CCE was
167 suppressed at both higher methane concentrations and higher temperatures (Fig. 4c and d) i.e., the exact
168 conditions induced by warming. In the ponds, therefore, the warmed methanotrophs would assimilate a

169 smaller fraction of their metabolised methane, grow less efficiently and thus lack the potential to reach the
170 required abundance to balance greater methane production. Whereas we cannot predict the increase in
171 methane production from a simple physiological response to warming, we could determine just such a
172 simple physiological response for methane oxidation. In contrast to warming-induced change in the
173 methanogen community, the methanotroph community was conserved (Supplementary Fig. 4 and
174 Supplementary Table 3); it is noticeable, however, that 11 of the 16 detected OTUs had a lower relative
175 abundance (with two genera being undetected) in the warmed ponds (Supplementary Table 5). We
176 propose that whereas warming makes hydrogenotrophic methanogenesis more favourable, thus changing
177 the methanogen community, there is no similar mechanism to favourably alter the methanotroph
178 community.

179 Our long-term warming experiment provides a mechanistic understanding of a potential positive
180 feedback warming loop in the freshwater methane cycle. In particular, warming increases the efficiency
181 of methanogenesis and preferentially alters hydrogenotrophy while limiting the capacity of
182 methanotrophs to consume methane by impaired growth, which, together, increase the global warming
183 potential of the carbon gases emitted. These emergent properties increase methane emissions far beyond a
184 simple physiological increase to warming alone and what we have witnessed under experimental warming
185 is, in part, borne out at the global-scale as a disproportionate increase in the capacity of a variety of
186 naturally warmer ecosystems (e.g. wetlands, croplands, forests and grasslands, *see* Methods) to emit more
187 methane. Together, our findings strongly indicate that as Earth continues to warm, natural ecosystems
188 will emit disproportionately more methane to the atmosphere in a positive feedback warming loop (Fig 5).

189 **Acknowledgments**

190 This study was supported by Queen Mary University of London and the U.K. Natural Environment
191 Research Council (NE/M02086X/1, NE/M020886/1). We thank Ian Sanders and Felicity Shelley for
192 technical and fieldwork assistance; James Pretty for mesocosm pond maintenance; Martin Rouen for

193 designing and installing the Campbell control and data-logging system; Hannah Prentice for collecting
194 sediments and DNA extraction; Chloe Economou and Monika Struebig for help with molecular work;
195 Patrick K.H. Lee for providing the *mcrA* database and related documents for bioinformatics analysis. We
196 thank the principal investigators of the methane flux data products including William Quinton, Oliver
197 Sonnentag, Georg Wohlfahrt, Sebastien Gogo, Ted Schuur, Ken Krauss, Ankur Desai, Gil Bohrer,
198 Rodrigo Vargas, Dennis Baldocchi, Jiquan Chen, Housen Chu, Hiroki Iwata, Masahito Ueyama and
199 Yoshinobu Harazono. We also thank the funding agencies that supported their flux measurements and the
200 three anonymous reviewers whose comments greatly improved the manuscript.

201 **Author contributions**

202 M.T., Y.Z. and K.J.P conceived the study and Y.Z. conducted the vast majority of the experiments and
203 analysed the data. Y.Z., M.T., K.J.P., G.Y.D. and A.J.D. discussed the data. Y.Z., M.T. and K.J.P. wrote
204 the manuscript and all authors contributed to revisions. Y.Z. and S.H. set up the chamber system. Y.Z.,
205 O.E. and L.S. performed molecular analyses.

206 **Competing interests**

207 The authors declare no competing financial interests.

208 **Additional Information**

209 **Supplementary information** and **Extended Data Figures** are available in the online version of the paper.

210 **Reprints and permissions information** is available at www.nature.com/reprints.

211 **Correspondence and requests for materials** should be addressed to M.T. (m.trimmer@qmul.ac.uk).

212

213 References

- 214 1. Nisbet, E. G., Dlugokencky, E. J. & Bousquet, P. Methane on the Rise--Again. *Science* **343**, 493–
215 495 (2014).
- 216 2. Balcombe, P., Speirs, J. F., Brandon, N. P. & Hawkes, A. D. Methane emissions: choosing the
217 right climate metric and time horizon. *Environ. Sci. Process. Impacts* **20**, 1323–1339 (2018).
- 218 3. Holgerson, M. A. & Raymond, P. A. Large contribution to inland water CO₂ and CH₄ emissions
219 from very small ponds. *Nat. Geosci.* **9**, 222–226 (2016).
- 220 4. Saunio, M. *et al.* The global methane budget 2000–2012. *Earth Syst. Sci. Data* **8**, 697–751 (2016).
- 221 5. Bridgman, S. D., Cadillo-Quiroz, H., Keller, J. K. & Zhuang, Q. Methane emissions from
222 wetlands: Biogeochemical, microbial, and modeling perspectives from local to global scales. *Glob.
223 Chang. Biol.* **19**, 1325–1346 (2013).
- 224 6. Gudas, C. *et al.* Temperature-controlled organic carbon mineralization in lake sediments. *Nature*
225 **466**, 478–481 (2010).
- 226 7. Yvon-Durocher, G. *et al.* Methane fluxes show consistent temperature dependence across
227 microbial to ecosystem scales. *Nature* **507**, 488–91 (2014).
- 228 8. Allen, A. P., Gillooly, J. F. & Brown, J. H. Linking the global carbon cycle to individual
229 metabolism. *Funct. Ecol.* **19**, 202–213 (2005).
- 230 9. Hanson, R. S. & Hanson, T. E. Methanotrophic bacteria. *Microbiol. Rev.* **60**, 439–471 (1996).
- 231 10. Shelley, F., Abdullahi, F., Grey, J. & Trimmer, M. Microbial methane cycling in the bed of a chalk
232 river: oxidation has the potential to match methanogenesis enhanced by warming. *Freshw. Biol.* **60**,
233 150–160 (2015).
- 234 11. Mohanty, S. R., Bodelier, P. L. E. & Conrad, R. Effect of temperature on composition of the
235 methanotrophic community in rice field and forest soil. *FEMS Microbiol. Ecol.* **62**, 24–31 (2007).
- 236 12. Høj, L., Olsen, R. A. & Torsvik, V. L. Effects of temperature on the diversity and community
237 structure of known methanogenic groups and other archaea in high Arctic peat. *ISME J.* **2**, 37–48
238 (2008).
- 239 13. Hall, E. K. *et al.* Understanding how microbiomes influence the systems they inhabit. *Nat.*
240 *Microbiol.* **3**, 977–982 (2018).
- 241 14. Ho, A., Lüke, C. & Frenzel, P. Recovery of methanotrophs from disturbance: Population dynamics,
242 evenness and functioning. *ISME J.* **5**, 750–758 (2011).
- 243 15. Rocca, J. D. *et al.* Relationships between protein-encoding gene abundance and corresponding
244 process are commonly assumed yet rarely observed. *ISME J.* **9**, 1693–1699 (2015).
- 245 16. Trimmer, M. *et al.* Riverbed methanotrophy sustained by high carbon conversion efficiency. *ISME*
246 *J.* **9**, 2304–2314 (2015).
- 247 17. Fey, A. & Conrad, R. Effect of Temperature on Carbon and Electron Flow and on the Archaeal
248 Community in Methanogenic Rice Field Soil. *Appl. Environ. Microbiol.* **66**, 4790–4797 (2000).
- 249 18. Ho, A. & Frenzel, P. Heat stress and methane-oxidizing bacteria: Effects on activity and
250 population dynamics. *Soil Biol. Biochem.* **50**, 22–25 (2012).

- 251 19. Wilson, R. M. *et al.* Stability of peatland carbon to rising temperatures. *Nat. Commun.* **7**, 1–10
252 (2016).
- 253 20. Yvon-Durocher, G., Hulatt, C. J., Woodward, G. & Trimmer, M. Long-term warming amplifies
254 shifts in the carbon cycle of experimental ponds. *Nat. Clim. Chang.* **7**, 209–213 (2017).
- 255 21. Yvon-Durocher, G. *et al.* Five Years of Experimental Warming Increases the Biodiversity and
256 Productivity of Phytoplankton. *PLoS Biol.* **13**, 1–22 (2015).
- 257 22. Davidson, T. A. *et al.* Synergy between nutrients and warming enhances methane ebullition from
258 experimental lakes. *Nat. Clim. Chang.* **8**, 156–160 (2018).
- 259 23. McCalley, C. K. *et al.* Methane dynamics regulated by microbial community response to
260 permafrost thaw. *Nature* **514**, 478–481 (2014).
- 261 24. Conrad, R. Contribution of hydrogen to methane production and control of hydrogen
262 concentrations in methanogenic soils and sediments. *FEMS Microbiol. Ecol.* **28**, 193–202 (1999).
- 263 25. Wilson, R. M. *et al.* Hydrogenation of organic matter as a terminal electron sink sustains high
264 CO₂:CH₄ production ratios during anaerobic decomposition. *Org. Geochem.* **112**, 22–32 (2017).
- 265 26. Liu, Y. & Whitman, W. B. Metabolic, Phylogenetic, and Ecological Diversity of the
266 Methanogenic Archaea. *Ann. N. Y. Acad. Sci.* **1125**, 171–189 (2008).
- 267 27. Hodgkins, S. B. *et al.* Changes in peat chemistry associated with permafrost thaw increase
268 greenhouse gas production. *Proc. Natl. Acad. Sci. U. S. A.* **111**, 5819–5824 (2014).
- 269 28. Glissmann, K., Chin, K. J., Casper, P. & Conrad, R. Methanogenic pathway and archaeal
270 community structure in the sediment of eutrophic Lake Dagow: Effect of temperature. *Microb.*
271 *Ecol.* **48**, 389–399 (2004).
- 272 29. Inglett, K. S., Inglett, P. W., Reddy, K. R. & Osborne, T. Z. Temperature sensitivity of greenhouse
273 gas production in wetland soils of different vegetation. *Biogeochemistry* **108**, 77–90 (2012).
- 274 30. Conrad, R., Klose, M. & Noll, M. Functional and structural response of the methanogenic
275 microbial community in rice field soil to temperature change. *Environ. Microbiol.* **11**, 1844–1853
276 (2009).
- 277 31. Metje, M. & Frenzel, P. Methanogenesis and methanogenic pathways in a peat from subarctic
278 permafrost. *Environ. Microbiol.* **9**, 954–964 (2007).
- 279 32. Nozhevnikova, A. N. *et al.* Influence of temperature and high acetate concentrations on
280 methanogenesis in lake sediment slurries. *FEMS Microbiol. Ecol.* **62**, 336–344 (2007).
- 281 33. Wen, X. *et al.* Global biogeographic analysis of methanogenic archaea identifies community-
282 shaping environmental factors of natural environments. *Front. Microbiol.* **8**, 1–13 (2017).
- 283 34. Conrad, R. *et al.* Stable carbon isotope discrimination and microbiology of methane formation in
284 tropical anoxic lake sediments. *Biogeosciences* **8**, 795–814 (2011).
- 285 35. Kotsyurbenko, O. R. Trophic interactions in the methanogenic microbial community of low-
286 temperature terrestrial ecosystems. in *FEMS Microbiology Ecology* vol. 53 3–13 (2005).
- 287 36. Yvon-Durocher, G., Montoya, J. M., Woodward, G., Jones, J. I. & Trimmer, M. Warming
288 increases the proportion of primary production emitted as methane from freshwater mesocosms.
289 *Glob. Chang. Biol.* **17**, 1225–1234 (2011).

290 37. Reim, A., Lüke, C., Krause, S., Pratscher, J. & Frenzel, P. One millimetre makes the difference:
291 High-resolution analysis of methane-oxidizing bacteria and their specific activity at the oxic-
292 anoxic interface in a flooded paddy soil. *ISME J.* **6**, 2128–2139 (2012).

293

294 **Figures**

295 **Fig. 1 | Ongoing divergence in methane emissions from the surface of our ponds mirrors natural**
296 **warming. a**, Emissions from our warmed and ambient ponds in 2007³⁶, 2013²⁰ and 2017 ($n=3553$, this
297 study) have continued to diverge beyond that predicted for their 4°C difference in temperature (black-
298 dashed line, equation 2, Methods). **b**, Ratio of CH₄ to CO₂ emitted at night ($n=4884$, *see* Methods) is 1.8-
299 fold higher with warming (t -statistic, ***: $p<0.001$). **c**, Our disproportionate increase in methane
300 emissions in 2017 (**a**), maps onto a trend of increasing capacity of naturally warmer ecosystems,
301 including wetlands, croplands and forests (*see* Methods) to emit more methane - standardised to 15°C.
302 Vertical and horizontal lines, 95% CI.

303

304 **Fig. 2 | Long-term warming increases methane production over methanogen abundance.** **a**, In the
305 laboratory ($n=238$, without additional substrates), warmed sediments produced more methane than
306 ambient sediments, standardised to 15°C. **b**, Production increased equally ($n=32$, $p=0.4$) with carbon
307 quality (k) in both treatments but warming stepped-up the fraction of carbon turned-over to methane
308 ($p<0.01$). **c**, Warming increased methanogen abundance (circles) and methanogen efficiency (activity,
309 triangles, $n=79$). **d**, Ratio of CH₄ to CO₂ produced by warmed sediments was ~3-fold higher than ambient
310 sediments ($n=218$). As ~95% of CH₄ is oxidised to CO₂ before emission from the ponds, the laboratory
311 CH₄ to CO₂ ratio is higher (Fig. 1b). Vertical lines, 95% CI. * $p<0.05$; ** $p<0.01$; *** $p<0.001$.

312 **Fig. 3 | Long-term warming provides a mechanism to selectively alter the methanogen community.**
313 **a**, Significant shifts in the methanogen community between ambient and warmed ponds ($n=79$, principal
314 coordinate analysis at genus level, *see* Methods) were due to **b**, significant shifts in the relative abundance
315 of two hydrogenotrophic genera (*Methanospirillum* and *Methanobacterium*). **c**, Hydrogen stimulated
316 methanogenesis in the warmed pond sediments above that for acetate ($n=662$, vertical lines, 95% CI,
317 statistical significance compared to the controls ******* and between the warmed and ambient ponds by *
318 between the means ($*p<0.05$, $**p<0.01$, $***p<0.001$)). **d**, Hydrogenotrophy is more sensitive to
319 temperature and warming makes hydrogenotrophy more favourable, selectively altering the methanogen
320 community.

321 **Fig. 4 | Methane oxidation is conserved and the growth of methanotrophy impaired under warming.**
322 **a**, Strong physiological response in methane oxidation to higher methane in the laboratory, with a
323 comparable capacity in warmed and ambient pond sediments ($n=158$, $p>0.05$ for V_{max} and k_m) and **b**, a
324 similarly conserved response to temperature ($n=192$, $p=0.068$). Methanotrophic growth efficiency (i.e.,
325 carbon conversion efficiency, CCE %) was impaired at **c**, higher methane concentrations ($n=69$, $p<0.01$)
326 and **d**, higher-temperatures ($n=191$, $p<0.01$) i.e., the conditions induced by warming in the ponds. Under
327 substrate limitation and impaired growth, the methanotroph community was conserved and lacked the
328 potential to reach the required abundance to balance the increase in methane production under warming.

329 **Fig. 5 | Positive climate warming feedback loop revealed by our long-term experiment.** Methane
330 emissions cannot be predicted by temperature alone and both the magnitude of emission and the ratio CH₄
331 to CO₂ increase as apparent emergent properties of changes in the overall methane cycle (red arrow).
332 Long-term warming favours hydrogenotrophic methanogenesis, providing a mechanism to alter both the
333 efficiency (yellow rectangle) and structure of the methanogen community (green rectangle). In contrast,
334 there is no similar mechanism to alter the methanotroph community and physiological responses
335 dominate. Methane oxidation cannot offset the extra methane production under warming (blue rectangle),
336 and a positive feedback loop in the methane cycle develops through global warming.

337

338 **Extended Data Figures**

339 **Extended Data Fig. 1 | Schematic of experimental pond set-up and dynamic chamber**

340 **measurements.** Twenty artificial ponds, with 10 warmed (red) by 4°C above 10 ambient (blue) ponds,
341 were paired in a randomized block design **(a)** and controlled via two temperature sensors (T1, T2), a
342 thermocouple (T-stat) and a solid-state relay (SSR) **(b)**. Dynamic LI-COR chambers, floating on
343 lifebuoys, were installed on 7 each of the warmed and ambient ponds **(c)**. Each floating chamber was
344 connected to one of the inlet ports on the MIU and the MIU outlet port was connected to the gas inlet port
345 of Ultra-Portable Greenhouse Gas Analyzer (LGR) **(d)**. A dynamic chamber is sequentially triggered to
346 close by customised Campbell control unit (CCU) for 30 minutes for gas measurements while the other
347 chambers remain open. When a chamber is triggered to close, the MIU switches simultaneously to the
348 inlet connected to the closing chamber to direct its gas flow to the LGR. *See Methods and Extended Data*
349 *Fig. 2 for further details on methane emissions.*

350

351 **Extended Data Fig. 2 | Consistent seasonal patterns in daily methane emissions under warming but**
352 **with ongoing divergence over 10 years (2007³⁶, 2013²⁰ and 2017 (this study)).** The seasonal patterns in
353 all 3 years are very similar, despite the use of different techniques but the frequent measurements (three
354 times daily) using dynamic chambers in 2017 captured far more details in emissions compared to 2007
355 and 2013 when static chambers were used to measure methane emission on 7 and 12 occasions over each
356 year, respectively. Note the natural log scale for methane emissions.

357

358

359 **Extended Data Fig. 3 | Methane emissions at night and during the day.** Methane emissions during the
360 day (a) and at night (b) follow the similar seasonal patterns; yet the methane emissions at night are
361 significantly greater than during the day (c).

362

363 **Methods**

364 **Mesocosm pond facility**

365 Twenty artificial ponds were installed in 2005 at the Freshwater Biological Association's River
366 Laboratory in Dorset, UK (2°10'W, 50°30'N). The ponds (1.8m diameter and 2.5m²) hold 1m³ of water
367 (50cm deep), have a 6-10cm layer of fine sand sediment and were seeded with local communities of
368 macroinvertebrates and plants to mimic shallow lakes^{20,21,36}. The ponds are arranged in a randomised-
369 block design, with half of the ponds being warmed by 4°C above ambient temperatures since 2006
370 (Extended Data Figure 1).

371 **Methane and carbon dioxide emissions from the surface of the ponds**

372 Methane and carbon dioxide emissions from the surface of the ponds were measured ~3 times per day
373 from February 2017 to February 2018 using a combination of an Ultra-Portable Greenhouse Gas Analyzer
374 (915-0011, LGR, Los Gatos Research), a Multi-port Inlet Unit (MIU, LGR), 14 dynamic chambers (Ø
375 20cm, 0.43L, 8100-101, LI-COR) and a customised Campbell control unit (CCU) (Extended Data Figure
376 1). Each dynamic chamber floats on a ring permanently fixed at the centre of 7 of the 10 warmed and 7 of
377 the 10 ambient ponds and are connected to 1 to 14 of the inlet ports on the MIU which is connected to the
378 inlet port of the LGR that pumps air at ~3 L min⁻¹. As the LGR cannot operate the dynamic chambers
379 directly, the CCU triggers them sequentially after receiving a signal from the LGR. Each chamber
380 remains open until triggered to close for a 30-minute sampling period, at which point the MIU switches to
381 the closing chamber to direct gas to the LGR. A complete cycle takes ~8h, including background
382 atmospheric methane. Between each chamber the CCU synchronizes the MIU and LGR to avoid any drift
383 in the sequence. Data were acquired at 1Hz and methane or carbon dioxide emissions calculated at
384 steady-state by³⁸:

$$F = \frac{(C_{\text{observation}} - C_{\text{background}})}{S_{\text{area}}} \times \frac{V_{\text{aeration}}}{dt} \quad (1)$$

385 Where F is the emission ($\mu\text{mol m}^{-2} \text{h}^{-1}$), $C_{\text{observation}}$ is the concentration of methane or carbon dioxide (μmol
386 L^{-1}) at steady-state (estimated by averaging the concentrations) and $C_{\text{background}}$ their respective atmospheric
387 concentrations ($\mu\text{mol L}^{-1}$), V_{aeration}/dt is the volume of air flowing through a chamber per hour and S_{area} is
388 the surface area of the chamber (0.031 m^2). We also needed to characterise ebullition events that lead to
389 rapid increases in methane concentrations over short periods of time and bias our emission estimates (*see*
390 Supplementary Fig. 6 for examples). Ebullition events were identified as a consistent increase in methane
391 concentrations over 5 seconds at a rate greater than 50ppb per second, to a maximum concentration, or
392 consistent decrease for 5 seconds, at a rate greater than 10ppb per second, after the post-ebullition
393 maxima. We acknowledge that these criteria also identify other non-steady flux events besides ebullition
394 and we subsequently distinguished these events from ebullition if their maximum methane concentration
395 was lower than atmospheric methane i.e., noise. Of the 16504 total chamber measurements, 198, i.e.,
396 1.2%, were identified as ebullition and 7, i.e., 0.04%, were identified as other non-steady-state events.
397 Both ebullition and other non-steady flux events were excluded from further calculations.

398 **Predicting methane emissions, production and oxidation from their apparent** 399 **activation energies**

400 Activation energy is a measure of temperature sensitivity^{7,8}. For example, the common activation energy
401 for methane emission of 0.96 eV, predicts a 1.70-fold increase in emissions under our 4°C warming
402 scenario according to:

$$\frac{R(T_W)}{R(T_A)} = e^{\frac{E_a}{kT_W} - \frac{E_a}{kT_A}} \quad (2)$$

403 Where $R(T)$ is the metabolic rate (e.g. methane emission and similarly for production or oxidation) and T_W
404 and T_A are the mean annual temperatures of the warmed and ambient ponds (288.15 and 292.15K,
405 respectively). k is the Boltzmann constant ($8.62 \times 10^{-6} \text{ eV K}^{-1}$).

406 **Potential methane production with temperature and additional substrates**

407 The pond setup provided 10 independent replicates for the warmed and ambient pond treatments
408 (Extended Data Figure 1). Three cores of intact sediment (typically 6cm to 10cm depth) were collected by
409 hand using small Perspex corers (\O 34mm \times 300mm) and butyl stoppers, every month from January,
410 2016, to December, 2016, (except for July) from three to five warmed and ambient ponds (4 on average),
411 selected randomly. Intact cores of sediment were stored in zip-lock bags and kept cool with freezer blocks
412 for transport back to laboratory (<4h) and then kept in the dark at 4°C.

413 Sub-samples (~3g) of the bottom sediment layers (below 4cm) from the same pond were homogenised,
414 thus no further pseudo-replication was included within each pond, and aliquoted into gas-tight vials (12ml,
415 Labco, Exetainer®) inside an anoxic glove box (CV204; Belle Technologies) filled with oxygen-free
416 nitrogen (OFN, BOC). The capacity and temperature sensitivity of methanogenic potentials with either
417 additional acetate or hydrogen as substrates were quantified. For acetate, pond water (3.6ml) and acetate
418 stock solutions (0.4ml, 100mM, Sigma-Aldrich®, for molecular biology) were flushed with OFN for 10
419 minutes and then added to each vial to create final concentrations of 10mM and the vials sealed. For
420 hydrogen, 4ml OFN-flushed pond water were added to each vial, the vials sealed and injected with 1ml of
421 the pure hydrogen (H_2 , research grade, BOC, Industrial Gases, Guilford, UK) to create an ~17% H_2
422 headspace (v/v). A further set of vials were left unamended as controls (see Supplementary Table 7 for
423 sample size). All the prepared vials were then incubated in separate batches at approximately 12°C, 17°C,
424 22°C and 26°C (precise temperature could vary by 2°C between months) for up to 4 days and shaken by
425 hand twice per day. The production of methane and carbon dioxide was quantified every 24h using a gas
426 chromatogram fitted with a hot-nickel methanizer and flame-ionization detector (Agilent Technology UK
427 Ltd., South Queensferry, UK), as before^{16,39}.

428 **Methane oxidation and its carbon conversion efficiency**

429 Three sediment cores were collected from 8 warmed and 8 ambient ponds using truncated syringes (25ml)
430 in May, June and July, 2017, to measure the temperature sensitivity and capacity of methane oxidation. In

431 December, 2018, three sediment cores were collected from the same ponds to measure the kinetic
432 concentration effect on methane oxidation rates. The sediment cores were kept cool and transported as
433 described above.

434 The top 2cm of sediment from each pond was homogenised and transferred into gas-tight vials (12ml,
435 Labco, Exetainer®) along with the overlying pond water (4ml). The vials then sealed to leave a headspace
436 of air. We quantified the effect of long-term warming on both the temperature and kinetic response of
437 methane oxidation. For temperature, we enriched the vials with 200µL of ¹³C-CH₄ (99% atom) to 40µmol
438 L⁻¹ in the water phase. Control vials were set up without ¹³C-CH₄ enrichment and all vials incubated with
439 gentle shaking (130 rpm) at 5°C, 10°C, 15°C and 22°C to mix the ¹³C-CH₄ throughout the slurry. Methane
440 concentrations described here are higher than in our ponds to enable short incubations (~22h) at the
441 different temperatures and avoid being confounded by substrate limitation (*see* kinetics). For the kinetic
442 response, the vials were enriched with ¹³C-CH₄ to 1 to 60 µmol L⁻¹ in the water phase and the vials
443 incubated as above at 22°C. Vials below 15µmol L⁻¹ ¹³C-CH₄ were incubated for <12h and those higher
444 initial incubated for ~20h when the experiments were fixed by injecting 200µL ZnCl₂ (50% w/v).

445 The carbon conversion efficiency of methanotrophy was estimated using the fraction of ¹³C-CH₄
446 recovered as ¹³C-inorganic carbon as per¹⁶: $1 - \frac{\Delta^{13}\text{C-inorganic}}{\Delta^{13}\text{C-CH}_4}$ where Δ represents the production of ¹³C-
447 inorganic or the consumption of ¹³C-CH₄.

448 **Oxygen profile measurements**

449 Dissolved oxygen concentrations in the water overlying the sediments were measured from October, 2015,
450 to October, 2016, in 7 warmed and 7 ambient ponds, using oxygen sensors (miniDOT oxygen logger,
451 PME, California USA) at 10 minute intervals. Penetration of oxygen into the sediments was measured in
452 April, 2016, at a resolution of 100µm, as described in⁴⁰.

453 **Statistical analysis**

454 All statistical analyses were performed in R (3.2.5)⁴¹.

455 **Annual methane emissions**

456 Rates of methane emission were natural log-transformed and fitted into Generalized additive mixed effect
457 models (GAMMs) to characterize the average annual emission patterns for the warmed or ambient ponds
458 as a fixed effect, as before²⁰. The annual rates of methane emissions were calculated using the parameter
459 estimates from the best GAMMs model (Supplementary Table 6) and extrapolated to a year by
460 multiplying by 365.

461 **Ratio of CH₄ to CO₂ emitted from the surface of the ponds and produced in anoxic** 462 **sediments**

463 Our artificial ponds are net sinks for CO₂^{20,21}. To illustrate the connection between our sediment potential
464 measurements for CH₄ and CO₂ production in the laboratory, we compared them to the emission ratio for
465 CH₄ and CO₂ from the ponds at night when they emitted both CH₄ and CO₂. Before statistical analysis,
466 the ratio data above the 95th percentiles for each treatment were characterized as outliers and removed.
467 The significance of the main treatment effect i.e., warmed or ambient ponds, was then determined using
468 the *t*-statistic.

469 **Meta-analysis on methane emission capacity across a natural temperature gradient**

470 There were 491 datasets available on the AmeriFlux (<http://ameriflux.lbl.gov/>) and EuroFlux network
471 (<http://www.europe-fluxdata.eu/>) (Supplementary Table 1). Of those, only 26 were for methane and air-
472 temperature and only 19 of the available sites covered at least 6 months of the year and demonstrated a
473 good relationship ($p < 0.05$) between methane emission and air-temperature. Half-hour aggregated eddy-
474 covariance data were downloaded for these 19 sites which are wetlands (68%), forests, grasslands and
475 shrubs (21%) and croplands (11%). The original methane emissions rates ($\text{nmol CH}_4 \text{ m}^{-2} \text{ s}^{-1}$) were then
476 integrated to give daily estimates of methane emissions ($\mu\text{mol CH}_4 \text{ m}^{-2} \text{ d}^{-1}$).

477 Daily rates of methane emission were then standardized to 15°C to provide comparable estimates of
478 methane emission capacities between sites using the Boltzmann-Arrhenius relationship:

$$\ln ME_i(T) = E_{ME} \left(\frac{1}{kT_{15}} - \frac{1}{kT_i} \right) + \ln ME(T_{15}) \quad (3)$$

479 Where $\ln ME_i(T)$ is the natural-logarithm-transformed rate of daily methane emissions by any site i ($i = 1,$
 480 $2, \dots, 19$) under air-temperature T in Kelvin. k is the Boltzmann constant and $\left(\frac{1}{kT_{15}} - \frac{1}{kT_i} \right)$ is standardized
 481 temperature for site i . T_{15} (15°C equals 288.15K) is the temperature used to center the temperature data.
 482 Therefore, the slope term E_{ME} represents the temperature sensitivity and the intercept $\ln ME(T_{15})$ is the
 483 estimated daily “capacity” of methane emission standardized to 15°C . The standardized methane emission
 484 capacities $\ln ME(T_{15})$ were then modelled as a simple linear function of annual average site temperatures
 485 using the “lm” function.

486 **Temperature sensitivity and capacity of methane production and oxidation**

487 We estimated the temperature sensitivity and capacity of methane production and oxidation using the
 488 Boltzmann-Arrhenius equation⁷:

$$\ln F_{ij}(T) = (\bar{E} + a_i + a_j) \left(\frac{1}{kT_C} - \frac{1}{kT_{ij}} \right) + (\overline{\ln F(T_C)} + b_i + b_j) \quad (4)$$

489 Where $F_{ij}(T)$ is the rate of methane production or oxidation by sediment from pond i ($i = 1, 2, \dots$),
 490 collected in month j ($j = 1, 2, \dots$). As our experimental design yielded replicate responses in ponds for both
 491 treatments over months, we treated sampling month and replicate pond as crossed random effects on the
 492 slope ($a_i + a_j$) and the intercept ($b_i + b_j$) of the models to account for the random variation among
 493 months and ponds from the fixed effect. Methane oxidation experiments were performed in only three
 494 months, therefore the parameter “sampling month” was not included to improve model convergence. The
 495 slope \bar{E} of equation (4) represents the estimated population activation energy (temperature sensitivity) in
 496 units of eV, for either methane production ($\overline{E_{MP}}$) or oxidation ($\overline{E_{MO}}$). k is the Boltzmann constant. We
 497 standardized the plot using the term $\frac{1}{kT_C}$, in which T_C (288.15K) is the average temperature in the ambient
 498 ponds *i.e.*, 15°C in 2017, so that the terms, $\overline{\ln F(T_C)}$ corresponds to the average capacity of methane

499 production or oxidation at T_C . The effect of treatment (i.e., ambient or warmed ponds) and substrates on
500 methane production, on both the slope (temperature sensitivity) and intercept (average capacity of
501 methane production or oxidation at T_C) were modelled as fixed effects.

502 The data were fitted into linear mixed-effect models (LMEM) using the lme4 package⁴². The details of
503 model fitting, selection and validation are provided in Supplementary Table 7 and 9 for production and
504 oxidation, respectively. After the best fitting model was determined, *post-hoc* pairwise comparisons of the
505 estimated marginal means of methane production capacity and temperature sensitivity were obtained
506 using the “emmeans” package⁴³.

507 **Turnover decay constants for organic carbon**

508 We derived turnover decay constants k (h^{-1}) as a relative indicator of sediment carbon quality⁴⁴:

$$k = \frac{R}{C} \quad (5)$$

509 Where R is the rate of CO_2 production standardized to 15°C ($\text{nmol g}^{-1} \text{h}^{-1}$) in anoxic slurry incubations and
510 C the concentration of organic carbon (nmol g^{-1}). To characterize the proportion of organic carbon
511 converted to methane in the sediments, we fitted k as an explanatory variable into a mixed effect model:

$$\ln MG_j = (\text{slope} + a_j) \times \ln k + (\text{intercept} + b_j) \quad (6)$$

512 Where $\ln MG_j$ is the natural logarithm of methane production capacity standardized to 15°C by any
513 sediment collected in month j ($j=1, 2, \dots$) and $\ln k$ is the natural logarithm of k . The slope represents the
514 potential to produce methane in response to carbon quality and the intercept the proportion of organic
515 carbon converted to methane, i.e., methane produced per unit carbon turned over. The random effect
516 terms a_j and b_j represent variation among sampling months. The effect of treatment (i.e., warmed or
517 ambient) on the intercept and slope were fitted into the model as a fixed effect and its significance tested
518 using the Likelihood Ratio Test (LRT) (Supplementary Table 8).

519 **Kinetic concentration effect on rates of methane oxidation**

520 The kinetic concentration effect on rates of CH₄ oxidation was characterised using a Michaelis-Menten
521 model:

$$MO_i(C_{CH_4}) = \frac{(V_{max} + a_i) \times C_{CH_4}}{(K_M + b_i) + C_{CH_4}} \quad (7)$$

522 Where MO_i is the rate of ¹³C-CH₄ oxidation by any sediment of pond i ($i=1, 2, \dots$). C_{CH_4} is the initial ¹³C-
523 CH₄ concentration. The parameters V_{max} and K_M were determined by fitting self-starting nonlinear mixed-
524 effect models. The mesocosm ponds were fitted into the models as random effects to account for their
525 variations on the parameter V_{max} (a_i) and on the parameter K_m (b_i) and the significance of warmed or
526 ambient ponds tested using LRT (Supplementary Table 9).

527 **Carbon conversion efficiency of methanotrophy**

528 To characterise temperature and kinetic effects on the carbon conversion efficiency (CCE), we fitted CCE
529 as a response variable into a mixed effect model:

$$CCE_i(T) = (slope + a_i) \times (T - T_C) + (\overline{CCE(T_C)} + b_i) \quad (8)$$

$$CCE_i(C_{CH_4}) = (slope + a_i) \times C_{CH_4} + (\overline{CCE(C_{CH_4,0})} + b_i) \quad (9)$$

530 Where $CCE_i(T)$ and $CCE_i(C_{CH_4})$ are the CCE (%) by any sediment from pond i ($i=1, 2, \dots$) at
531 temperature T or with an initial concentration of ¹³C-CH₄ C_{CH_4} . To quantify the temperature sensitivity,
532 again, we centered the plot to the average annual temperature in the ambient ponds (15°C), so that the
533 term $\overline{CCE(T_C)}$ represents the average CCE at 15°C. However, we did not center equation (9) and the
534 intercept term $\overline{CCE_i(C_{CH_4,0})}$ is the CCE estimate at 0 μmol L⁻¹. The random effect terms a_i and b_i represent
535 variation among ponds and the effect warmed or ambient ponds on the intercept and slope were fitted and
536 tested as above (Supplementary Table 10).

537 **Microbial community analysis**

538 **Sediment sampling and DNA extraction**

539 Monthly sediment samples were collected from March 2016 to August 2017 from 8 warmed and 8
540 ambient ponds using cut-off 25mL syringes. The top 2cm of sediment was transferred into an Eppendorf
541 tube and the rest into a Falcon tube and stored at -80°C. DNA was extracted from 0.5g of wet sediment
542 (DNeasy[®] PowerSoil[®] Kit; Qiagen) and DNA yield quantified using NanoDrop (Thermo Scientific)
543 according to manufacturer's instructions; yield was 1-4 µg g⁻¹ wet sediment.

544 **PCR amplification and sequencing**

545 The *mcrA* gene, a methanogen molecular marker, was amplified using *mcrIRD* primers⁴⁵ (forward: 5'-
546 TWYGACCARATMTGGYT-3'; reverse: 5'-ACRTTCATBGCRARTT-3'). PCRs were performed in
547 50µL containing 25µL of MyTaq[™] Red Mix (Bioline), 1µL of each primer (10µM), 3µL of DNA
548 template and 20µL of molecular biology quality water. Amplifications were performed in a T100[™]
549 Cyclor (Bio-Rad) following the thermal program: (1) 95°C for 5 min, (2) 40 cycles at 95°C for 45s, 51°C
550 for 45s and 72°C for 60s, (3) 72°C for 5min.

551 The *pmoA* gene, a methanotroph molecular marker, was amplified using a semi-nested PCR with A189F
552 (5'-3': GGNGACTGGGACTTCTGG) - A682R(5'-3': GAASGCNGAGAAGAASGC) in the first round
553 and A189F (5'-3': GGNGACTGGGACTTCTGG) - A650R (5'-3': ACGTCCTTACCGAAGGT) in the
554 second round⁴⁶. PCRs were performed in 25 µL containing: 12.5µL of MyTaq[™] Red Mix (Bioline), 1µL
555 of each primer (10µM), 1µL of DNA and 9.5µL of molecular biology quality water. For the first round, a
556 touch-down PCR⁴⁶ was performed in a T100[™] Cyclor (Bio-Rad) following the thermal program: (1)
557 94°C, 3 min, (2) 30 cycles at 94°C, 45 s, 62 to 52°C, 60 s (initially decreasing by 0.5°C per cycle down to
558 52°C) and 72°C, 180s, (3) 72 °C, 10 min. The second round followed the thermal program: (1) 94 °C, 3
559 min, (2) 22 cycles at 94 °C, 45 s, 56 °C, 60 s and 72 °C, 60 s, (3) 72 °C, 10 min. PCR products were
560 checked by agarose gel electrophoresis and stained with GelRed[®].

561 Before sequencing, PCR products were cleaned using Agencourt[®] AMPure[®] XP beads (Beckman
562 Coulter). Barcodes and linkers were added by a 10-cycle PCR (95°C, 3 min, 10 cycles of 98°C, 20s, 55°C,
563 15s and 72°C, 15s, 72°C, 5min). Final PCR products were quantified with a Qubit 2.0 Fluorometer
564 (Invitrogen). 250 ng of PCR product from each sample was normalised to 4 nmoles (SequalPrep
565 Normalization Plate Kit, Invitrogen) and combined for sequencing on the Illumina MiSeq platform (300
566 bp paired-end) at the Genomics Service, University of Warwick (UK).

567 **Processing of sequence data**

568 Downstream sequence analysis was conducted using QIIME2 (2018.2.0)⁴⁷ on the Apocrita HPC facility at
569 Queen Mary University of London, supported by QMUL Research-IT⁴⁸. Paired-end de-multiplexed files
570 were imported into QIIME2 and processed using DADA2 for modelling and correcting amplicon errors⁴⁹.
571 Primer sequences were trimmed, low-quality sequences (QS <35) and chimeras were removed. Amplicon
572 Sequence Variants (ASVs) were then inferred by DADA2. To analyse the data at genus-level, ASVs were
573 clustered first into species-level Operational Taxonomic Units (OTUs) at 85% similarity for *mcrA* and 90%
574 for *pmoA* sequences^{50,51}. OTUs were named using the pre-trained Naïve Bayes classifier using custom
575 databases^{52,53} to specific genus-level clusters (Supplementary Table 4 and 5). The classifier was trained on
576 sequences extracted for the appropriate *mcrA* and *pmoA* gene fragments.

577 One *mcrA* sample was not analysed as it contained too few sequence reads. The final dataset contained 68
578 unique *mcrA* OTUs from 1,633,993 reads and 65 unique *pmoA* OTUs from 2,013,666 reads.

579 **Phylogenetic analysis**

580 Classified sequence data was further analysed using “phyloseq” in R⁵⁴.

581 **Variation in richness (α -diversity)**

582 For each sample, OTU richness, Chao1 index, Shannon’s diversity index and evenness were calculated.

583 The differences between treatments were determined using mixed effect models, fitting each experimental

584 pond as a random effect. To test the significance of long-term warming on α -diversity LRT was
585 performed comparing full and reduced models (Supplementary Fig. 2 and 5).

586 **Variation in community composition (β -diversity)**

587 Principal Coordinate Analysis (PCoA) was used to analyse the communities between treatments using a
588 Bray-Curtis dissimilarity index with Hellinger standardized datasets at genus level. The scores of the
589 samples along the PCoA axes, with the two largest eigenvalues, were fitted into mixed-effect model and
590 the significance of long-term warming on scores was tested as above⁴² (Supplementary Table 3).

591 PERMANOVA⁵⁵ with the “adonis” function (vegan package)⁵⁶ was used to partition variation in a
592 distance matrix between treatments using a permutation test with pseudo-*F* ratios with similar results to
593 the PCoA.

594 **Differences in taxonomic abundance**

595 Changes in abundance under warming was investigated using a negative binomial generalized linear
596 model using DESeq2⁵⁷. DESeq2 was designed for RNA-seq data but has been used to analyse
597 microbiome data⁵⁷ especially if libraries are evenly sized. Change under warming at genus level was
598 estimated by setting the false discovery rate to 0.01.

599 **Quantitative PCR (qPCR) of methanogens and methanotrophs.**

600 Methanogen and methanotroph population sizes in sediment DNA samples was determined using qPCR
601 with the mcrIRD primers (*mcrA*) and A189F-A650 primers (*pmoA*), respectively. Amplifications were
602 performed using CFX384 TouchTM Real-Time PCR (Bio-Rad) in a total volume of 10 μ L containing: 5 μ L
603 of SsoAdvancedTM Universal SYBR[®] Green Supermix (Bio-Rad), 0.2 μ L of each primer (10 μ M), 1 μ L of
604 DNA template and 3.6 μ L of molecular biology quality water. Standard curves (10²-10⁷ copies μ L⁻¹) were
605 constructed by serial diluting plasmid DNA containing *mcrA* or *pmoA* gene inserts.

606 The qPCR program for *mcrA* was: (1) 98°C, 3min; (2) 40 cycles at 98°C, 15s, 55°C, 15s and 72°C,
607 60s; (3) 95°C, 10s and for *pmoA* was: (1) 96°C, 5min; (2) 40 cycles at 94°C, 45s, 60°C, 45s and at
608 72°C, 45s. Products specificity and size were confirmed by melt curve analysis after the final
609 extension.

610 **Cell-specific activities of methanogens and methanotrophs**

611 Cell-specific activities were calculated for both methanogens and methanotrophs by dividing CH₄
612 production and oxidation capacity at 15°C by *mcrA* and *pmoA* gene copy abundances respectively.

613

614 **Data availability.**

615 The data that support the findings of this study are available from the corresponding author upon request.

616 DNA sequences are in the National Center for Biotechnology Information database, under BioProject ID
617 PRJNA484117.

618

619 38. Yver Kwok, C. E. *et al.* Methane emission estimates using chamber and tracer release experiments
620 for a municipal waste water treatment plant. *Atmos. Meas. Tech.* **8**, 2853–2867 (2015).

621 39. Sanders, I. A. *et al.* Emission of methane from chalk streams has potential implications for
622 agricultural practices. *Freshw. Biol.* **52**, 1176–1186 (2007).

623 40. Neubacher, E. C., Parker, R. E. & Trimmer, M. Short-term hypoxia alters the balance of the
624 nitrogen cycle in coastal sediments. *Limnol. Oceanogr.* **56**, 651–665 (2011).

625 41. R Core Team. R: A Language and Environment for Statistical Computing. (2014).

626 42. Kuznetsova, A., Brockhoff, P. B. & Christensen, R. H. B. {lmerTest} Package: Tests in Linear
627 Mixed Effects Models. *J. Stat. Softw.* **82**, 1–26 (2017).

628 43. Lenth, R. emmeans: Estimated Marginal Means, aka Least-Squares Means. (2019).

629 44. Nicholls, J. C. & Trimmer, M. Widespread occurrence of the anammox reaction in estuarine
630 sediments. *Aquat. Microb. Ecol.* **55**, 105–113 (2009).

631 45. Lever, M. A. & Teske, A. P. Diversity of methane-cycling archaea in hydrothermal sediment
632 investigated by general and group-specific PCR primers. *Appl. Environ. Microbiol.* **81**, 1426–1441
633 (2015).

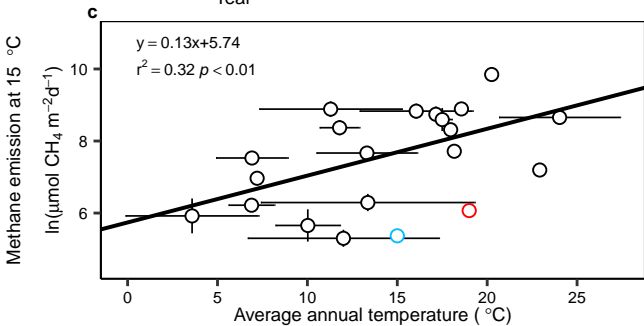
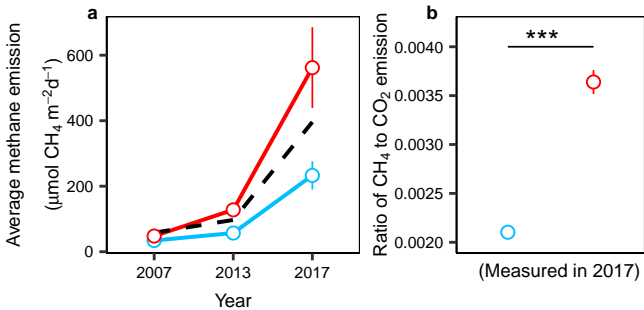
634 46. Horz, H. P., Rich, V., Avrahami, S. & Bohannon, B. J. M. Methane-oxidizing bacteria in a

- 635 California upland grassland soil: Diversity and response to simulated global change. *Appl. Environ.*
636 *Microbiol.* **71**, 2642–2652 (2005).
- 637 47. Caporaso, J. G. *et al.* QIIME allows analysis of high-throughput community sequencing data. *Nat.*
638 *Methods* **7**, 335–336 (2010).
- 639 48. King, T., Butcher, S. & Zalewski, L. Apocrita - High Performance Computing Cluster for Queen
640 Mary University of London. (2017) doi:10.5281/ZENODO.438045.
- 641 49. Callahan, B. J. *et al.* DADA2: High-resolution sample inference from Illumina amplicon data. *Nat.*
642 *Methods* **13**, 581–583 (2016).
- 643 50. Pester, M., Friedrich, M. W., Schink, B. & Brune, A. *pmoA*-based analysis of methanotrophs in a
644 littoral lake sediment reveals a diverse and stable community in a dynamic environment. *Appl.*
645 *Environ. Microbiol.* **70**, 3138–3142 (2004).
- 646 51. Oakley, B. B., Carbonero, F., Dowd, S. E., Hawkins, R. J. & Purdy, K. J. Contrasting patterns of
647 niche partitioning between two anaerobic terminal oxidizers of organic matter. *ISME J.* **6**, 905–
648 914 (2012).
- 649 52. Wilkins, D., Lu, X. Y., Shen, Z., Chen, J. & Lee, P. K. H. Pyrosequencing of *mcrA* and archaeal
650 16s rRNA genes reveals diversity and substrate preferences of methanogen communities in
651 anaerobic digesters. *Appl. Environ. Microbiol.* **81**, 604–613 (2015).
- 652 53. Yang, Sizhong; Wen, Xi; Liebner, S. *pmoA* gene reference database (fasta-formatted sequences
653 and taxonomy). *GFZ Data Services* (2016).
- 654 54. McMurdie, P. J. & Holmes, S. phyloseq: An R Package for Reproducible Interactive Analysis and
655 Graphics of Microbiome Census Data. *PLoS One* **8**, e61217 (2013).
- 656 55. Anderson, M. J. Permutational Multivariate Analysis of Variance (PERMANOVA). in *Wiley*
657 *StatsRef: Statistics Reference Online* 1–15 (Wiley, 2017).
- 658 56. Oksanen, J. *et al.* *vegan*: Community Ecology Package. (2018).
- 659 57. Love, M. I., Huber, W. & Anders, S. Moderated estimation of fold change and dispersion for
660 RNA-seq data with DESeq2. *Genome Biol.* **15**, 550 (2014).

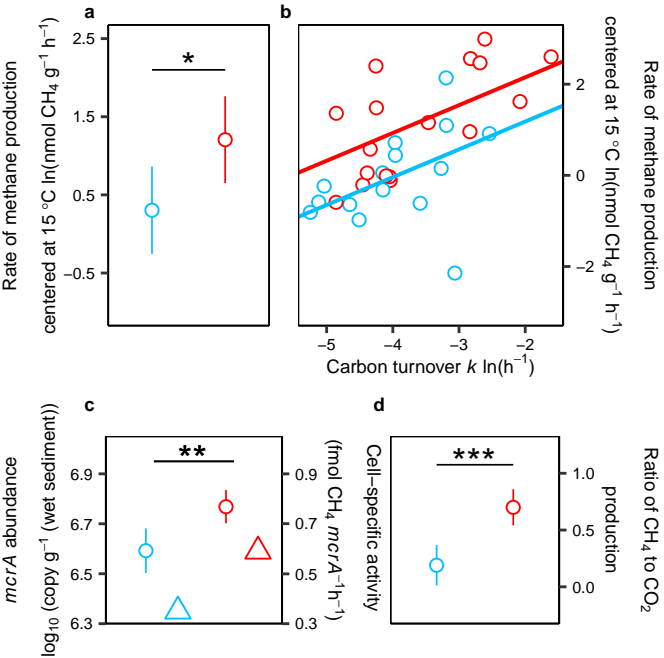
661

662

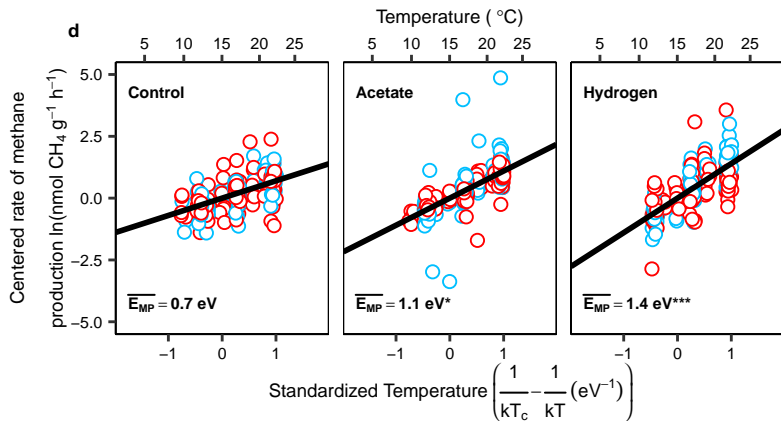
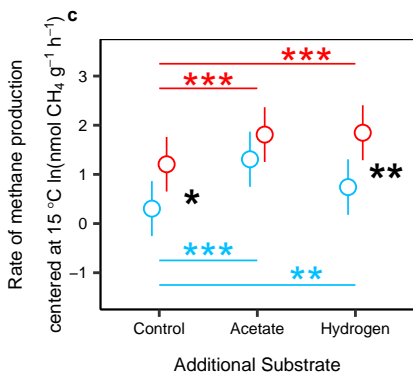
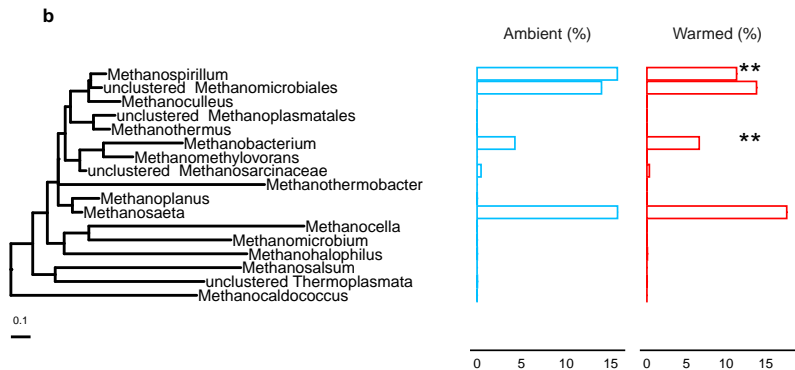
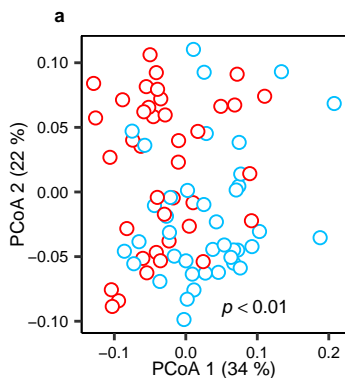
Treatment ○ Ambient ponds ○ Warmed ponds ○ Natural ecosystems



Treatment ○ Ambient ponds ○ Warmed ponds

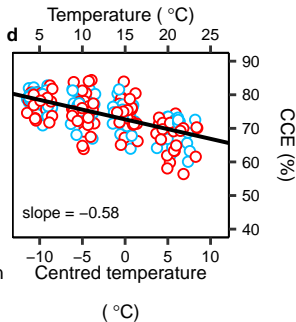
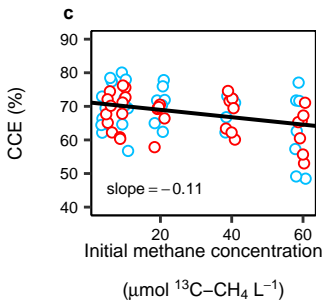
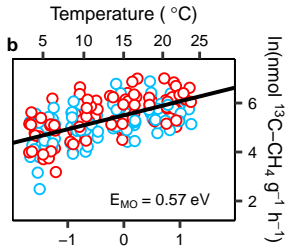
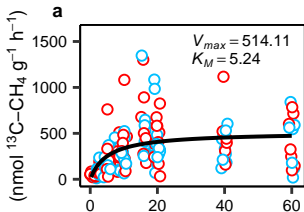


Treatment ○ Ambient ponds ○ Warmed ponds



Treatment ○ Ambient ponds ○ Warmed ponds

Rate of oxidation



✘ Predict 1.7-fold increase in CH₄ emission if temperature increases by 4 °C

